

## Article

# Use of RPA Images in the Mapping of the Chlorophyll Index of Coffee Plants

Luana Mendes dos Santos<sup>1</sup> , Gabriel Araújo e Silva Ferraz<sup>1,\*</sup> , Milene Alves de Figueiredo Carvalho<sup>2</sup> ,  
Sabrina Aparecida Teodoro<sup>1</sup>, Alisson André Vicente Campos<sup>3</sup> and Pedro Menicucci Neto<sup>3</sup>

<sup>1</sup> Agricultural Engineering Department, Federal University of Lavras, Lavras 37200-000, Minas Gerais, Brazil

<sup>2</sup> Embrapa Café, Brasília 70770-901, Distrito Federal, Brazil

<sup>3</sup> Department of Agronomy/Phytotechnics, Federal University of Lavras,  
Lavras 37200-000, Minas Gerais, Brazil

\* Correspondence: gabriel.ferraz@ufla.br

**Abstract:** Coffee trading is an important source of income for the Brazilian commercial balance. Chlorophyll (Chl) are pigments responsible for converting radiation into energy; these pigments are closely related to the photosynthetic efficiency of plants, and the evaluation of the nutritional status of the coffee tree. The inversion method can be used for estimating the canopy chlorophyll content ( $Chl_{canopy}$ ) using the leaf chlorophyll content ( $Chl_{leaf}$ ) and the leaf area index (LAI). The application of vegetation indices (VIs) in high spatial resolution images obtained from remotely piloted aircraft (RPA) can assist in the characterization of  $Chl_{canopy}$  in addition to providing vital and fast information for monitoring crops and aiding decision-making. This study aimed to identify which VIs adequately explain the Chl and evaluate the relationships between the VIs obtained from remotely piloted aircraft (RPA) images and the  $Chl_{leaf}$  and  $Chl_{canopy}$  in coffee plants during the wet and dry seasons. The experiment was conducted on a *Coffea arabica* L. plantation in Lavras, Minas Gerais, Brazil. Images were collected on 26 November 2019 (wet), 11 August 2020 (dry), and 26 August 2021 (dry) by a multispectral camera embedded in a quadcopter. Plant height (H), crow diameter (D), and  $Chl_{leaf}$  (a, b and total) data were collected in the field by a metre ruler (H and D) and sensor ( $Chl_{leaf}$ ). The LAI was calculated based on H and D. The  $Chl_{canopy}$  (a, b, and total) was calculated based on  $Chl_{leaf}$  and LAI. The image processing was performed in Pix4D software, and postprocessing and calculation of the 21 VIs were performed in QGIS. Statistical analyses (descriptive, statistical tests, Pearson correlation, residuals calculation, and linear regression) were performed using the software R. The VIs from the RPA that best correlates to  $Chl_{canopy}$  in the wet season were the Modified Chlorophyll Absorption Ratio Index 2 ( $MCARI2_{RPA}$ ), Modified Simple Ratio ( $MSR_{RPA}$ ) and Simple Ratio ( $SR_{RPA}$ ). These VIs had high sensitivity and, therefore, were more affected by chlorophyll variability. For the two dry season studied days, there were no patterns in the relationships between  $Chl_{leaf}$ ,  $Chl_{canopy}$ , and the VIs. It was possible to use the Chl inversion method for the coffee during the wet season.

**Keywords:** unmanned aircraft systems; canopy chlorophyll content; *Coffea arabica* L.



**Citation:** Santos, L.M.d.; Ferraz, G.A.e.S.; Carvalho, M.A.d.F.; Teodoro, S.A.; Campos, A.A.V.; Menicucci Neto, P. Use of RPA Images in the Mapping of the Chlorophyll Index of Coffee Plants. *Sustainability* **2022**, *14*, 13118. <https://doi.org/10.3390/su142013118>

Academic Editor: Antonio Miguel Martínez-Graña

Received: 18 August 2022

Accepted: 7 October 2022

Published: 13 October 2022

**Publisher's Note:** MDPI stays neutral with regard to jurisdictional claims in published maps and institutional affiliations.



**Copyright:** © 2022 by the authors. Licensee MDPI, Basel, Switzerland. This article is an open access article distributed under the terms and conditions of the Creative Commons Attribution (CC BY) license (<https://creativecommons.org/licenses/by/4.0/>).

## 1. Introduction

The estimated global coffee production for the 2022/23 harvest included 7.8 million 60-kg bags, more than the previous year [1]. Brazil is a major world producer of coffee, it is expected for the marketing year 2022/2023 to produce 64.3 million 60-kg bags, an increase of eleven percent compared to the last crop [1]. These numbers make Brazil the major world producer [1]. In this context, coffee is of commercial importance for Brazilian income because it is an agricultural commodity and a source of income for family farmers in this country.

However, there is growing evidence that farmers are facing challenges in coffee production due to climate change in the main coffee-producing regions, such as southern

Minas Gerais state, which experienced rainfall below the historical average [2] and increased incidence and severity of pests and diseases [3,4]. Faced with these challenges, production costs increased, and there was a reduction in bean quality and quantity. According to Chemura et al. [5], coffee crops have significant input costs and require intra- and inter-seasonal evaluations of crop conditions and monitoring of crop status and productivity to achieve profitability and sustainable production.

Coffee plants' morphological and physiological parameters are good indicators of vegetation conditions and assist in crop monitoring. It is possible to cite plant height, canopy diameter, and leaf area index (LAI) as morphological parameters [6,7]. Additionally, it is possible to highlight chlorophyll (Chl) as a physiological parameter [5,8]. Furthermore, the climate could affect the coffee field in different ways. In the wet season, the high intensity of rainfall could cause high humidity, eventually resulting in the increased emergence of various diseases, and in the dry season, the plants can be subjected to accelerated evapotranspiration [8]. Thus, the season will affect the coffee plant and its morphological and physiological parameters.

The primary photosynthetic pigments in plants are chlorophyll a and b, and carotenoids (carotenes and xanthophylls). These pigments absorb energy at different wavelengths [9] and can vary from crop to crop [10]. This makes it possible to use remote sensing techniques to observe this characteristic in different crops. According to Santos et al. [11], photosynthetic pigments play an essential role in plant physiology, in addition to being correlated with concentrations of nitrogen (N) and foliar magnesium (Mg). Therefore, it can be considered that among the photosynthetic pigments, the chlorophyll content of the leaf is an indicator that represents the state of growth of the crops and is crucial for agricultural practices [12].

Plants' chlorophyll content can be measured by equipment such as chlorophyll metres, optical sensors and multispectral sensors [13] directly in the field, which can be labour intensive and time-consuming. The chlorophyll metre usually measures chlorophyll a, b, and total. Chlorophyll a (Chl a) is a pigment present in all organisms that perform oxygenic photosynthesis, and it is used to carry out photochemistry (the first stage of the photosynthetic process) [14]. Chlorophyll b (Chl b) is a ubiquitous accessory pigment in land plants, green algae, and prochlorophytes, and its biosynthesis is important in the plant's adaptation to various light environments [15].

Recent remote sensing studies, using new technologies such as remotely piloted aircraft (RPA), have shown a different view of crop fields, serving as the farmer's eye in the sky, facilitating the spread of this technology in the field. According to Salami et al. [16], RPA technology represents a paradigm shift. Unlike satellite images and airborne surveys, the images obtained by RPA have a high spatial resolution (in centimetres and even millimetres) and high temporal resolution (for example, several times a day) in addition to low operational cost, serving as a complement to the existing technologies, favouring precision agriculture and precision coffee farming. More advantages and disadvantages of these two platforms can be seen in studies of [17–19].

However, the transfer of empirical algorithms from satellite images to RPA images is a challenge, especially in spatial resolution, since RPA images are highly detailed, affecting the importance of structural parameters such as obtaining the Chl content [10]. The radiative transfer model (RTM) developed by [20] is widely used to generate reflectance from the canopy top, considering biophysical variables measured from the crop of interest. It is a combination of the leaf-level and canopy-level models, as described by [21]. It has been used with different degrees of success for a wide variety of vegetation types, such as poplar trees [22], beets [23], cotton [24], eucalyptus [25], pastures [26], maize [10,23] and forest canopies [27].

Nonetheless, this method has not been applied to data obtained from RPA images of coffee plantations. The chlorophyll inversion method to estimate the Chl content of the canopy ( $Chl_{canopy}$ ) uses the chlorophyll content of the leaf ( $Chl_{leaf}$ ) and the LAI, as

described by [10,28]. So the  $Chl_{canopy}$  can be calculated by  $Chl_{leaf} \times LAI$  [10,28]. The LAI can be calculated based on the canopy diameter and plant height, as described by [29].

Linked to this chlorophyll inversion method, in the context of remote sensing, using a vegetation index (VI) that characterizes the  $Chl_{canopy}$  is relevant. The VIs consist of a combination of two or more spectral bands, which allows monitoring and detecting changes in the crop from each crop's spectral response in its phenology. Many different VIs developed can explain or be correlated to one or more variables. According to Ahmad et al. [30], VIs provide vital information for crop monitoring and decision making and serve as a guide while planning to collect crop-specific data. With VIs, it is possible to map an area and see its spatial variability. Thus, correlating chlorophyll information with VIs can be interesting since it will be possible to see the spatial variability of the field. Moreover, it can be less time-consuming than field collecting sampling points.

This study hypothesises that high-spatial-resolution images obtained from RPA can be used to estimate the coffee canopy's chlorophyll content based on different VIs. Furthermore, this estimate is expected to be improved using the inversion/transformation of  $Chl_{leaf}$  into  $Chl_{canopy}$ . Thus, the objective of this study was to identify which VIs adequately explain the Chl inversion method and evaluate the relationships between the VIs obtained from the RPA images and the  $Chl_{leaf}$  and  $Chl_{canopy}$  indices of coffee plants in the wet and dry seasons.

## 2. Materials and Methods

### 2.1. Study Site and Field Data Collection

The study was conducted on an experimental coffee plantation (*Coffea arabica* L.) in Lavras, Minas Gerais, Brazil (21°13'36.47" S, 44°57'40.35" W) (Figure 1). The plantation belongs to the Department of Agriculture of the Federal University of Lavras (Universidade Federal de Lavras—UFLA) and contains experimental treatments related to water optimisation in coffee production, described in [31,32]. The plantation has an area of 0.48 ha and contains coffee plants of the “Mundo Novo 379-19” cultivar that were planted in January 2016, with spacings of 3.6 m between planting rows and 0.75 m between plants.

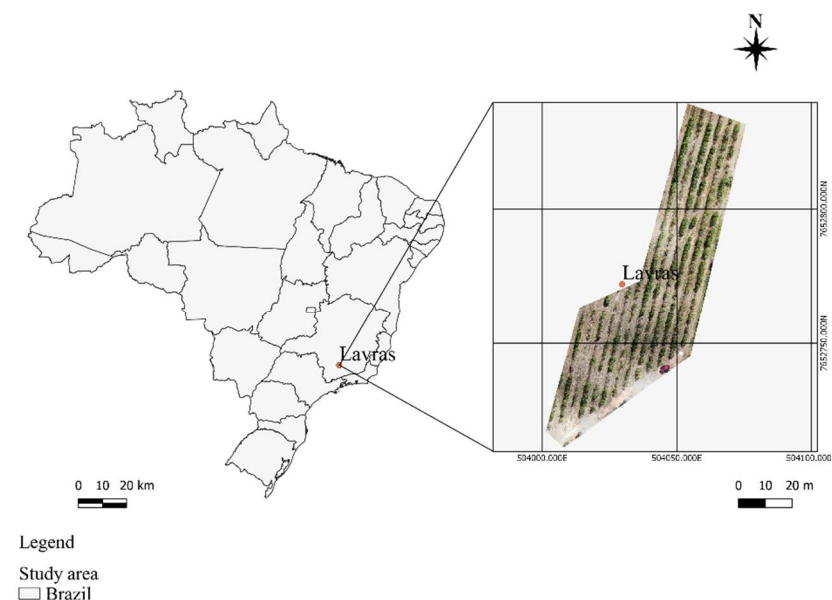


**Figure 1.** Study site location.

A total of 90 experimental plots were used. Each experimental plot consisted of six plants, and the four central plants were considered the useful plants. Between the treatment rows, a border row was used to avoid interference. The study site, the sampled plots and control points were georeferenced with the aid of a differential global positioning

system (DGPS) (Trimble Navigation Limited, Sunnyvale, CA, USA) with horizontal and vertical accuracy of 0.007 m.

## 2.2. RPA Data Collection

To collect the RPA spectral data on the coffee plantation, a quadcopter (Matrice 100, DJI) (Figure 2a) was used as the RPA platform. This quadcopter has four motors powered by a remotely controlled battery.



**Figure 2.** Equipment: (a) Matrice 100 quadcopter used for the survey; (b) Parrot Sequoia™ camera (image and irradiance sensors); (c) camera calibration target; (d) example of the control points.

The quadcopter used was a robust RPA and was controlled through an automated flight plan using the Precision Flight application installed on a smartphone. The flight plan was configured for an altitude of 30 m above ground level, with 80% overlap and sidelap and a speed of 3 m/s, following the method of Santos et al. (2020) [6]. Thus, a spatial resolution of 0.03 m pixel<sup>-1</sup> was achieved.

The RPA had a damping structure for camera stabilisation, oriented perpendicular to the ground, to which was coupled a Parrot Sequoia multispectral camera with five image sensors, including one 16-megapixel red, green, blue (RGB) visible sensor and four 1.2-megapixel sensors: green, red, red edge, and near infrared (NIR) (details in Table 1 and Figure 2b). However, the green, red, red edge, and NIR bands were used in this study.

**Table 1.** Parrot Sequoia Camera Specifications.

Camera	Parrot Sequoia™
Weight	107 g
Dimensions	5.9 × 4.1 × 2.9 cm
Spectral range	Green (0.53–0.57 μm), red (0.64–0.68 μm), red edge (0.73–0.74 μm), and near infrared (NIR) (0.77–0.81 μm)

Three flights were performed at different times: the first on 26 November 2019 (wet season), the second flight on 11 August 2020, and the third flight on 26 August 2021, both in the dry season. The multispectral images were collected around noon, under clear and sunny skies, to minimise the effects of clouds and the generation of shadows in the images. Before each flight, a radiometric calibration panel was used, in which images were taken with the camera that were subsequently used to calibrate the images captured over the area (Figure 2c).

The images were processed using the educational version of Pix4Dmapper Pro version 4.8 software (PIX4D SA, Prilly, Switzerland), following the processing workflow available in the software, in which the photos were calibrated and geometrically aligned to build the point cloud, 3D model, digital terrain model (DTM), digital surface model (DSM), and orthomosaic.

The orthomosaics were georeferenced in QGIS software version 3.10 (Quantum GIS) in the Universal Transverse Mercator (UTM) cartographic projection in the Sistema de Referencia Geocéntrico para Las Américas (SIRGAS) 2000 datum, zone 23 South, performing a first-order polynomial transformation with the nearest-neighbour resampling method, using six control points (Figure 2d) distributed in the area.

VIs are calculated based on the combination of spectral bands; they are commonly used as important indicators to monitor growth and predict yields, among other applications. In this study, 21 VIs were calculated, as described in Table 2. These VIs were obtained by averaging the useful plants using the QGIS zonal statistics tool.

**Table 2.** Vegetation indices obtained from the reflectance of the multispectral bands of the RPA images.

Vegetation Index	Equation	Source
Canopy Chlorophyll Content Index (CCCI)	$CCCI = \frac{NDRE}{NDVI}$	[33]
CI <sub>green</sub>	$CI_{green} = \left( \frac{\rho_{NIR}}{\rho_{green}} \right) - 1$	[34]
CI <sub>red edge</sub>	$CI_{red\ edge} = \left( \frac{\rho_{NIR}}{\rho_{red\ edge}} \right) - 1$	[34]
Enhanced Vegetation Index 2-Green (EVI2 <sub>green</sub> )	$EVI2_{green} = \frac{2.5 \times (\rho_{green} - \rho_{red})}{\rho_{green} + 2.4 \times \rho_{red} + 1}$	[35]
First Modified Chlorophyll Absorption Ratio Index (MCARI <sub>1</sub> )	$MCARI_1 = 1.2 \left[ 2.5(\rho_{NIR} - \rho_{green}) - 1.3(\rho_{NIR} - \rho_{green}) \right]$	[36]
Second Modified Chlorophyll Absorption Ratio Index (MCARI <sub>2</sub> )	$MCARI_2 = \frac{1.5 \left[ 2.5(\rho_{NIR} - \rho_{red}) - 1.3(\rho_{NIR} - \rho_{green}) \right]}{\sqrt{2(\rho_{NIR} + 1)^2 - (6\rho_{NIR} - 5\sqrt{\rho_{red}}) - 0.5}}$	[36]
Green Minus Red (GMR)	$GMR = \rho_{green} - \rho_{red}$	[37]
Green Normalized Difference Vegetation Index (GNDVI)	$GNDVI = \frac{\rho_{NIR} - \rho_{green}}{\rho_{NIR} + \rho_{green}}$	[38]
Modified Triangular Vegetation Index 1 (MTVI <sub>1</sub> )	$MTVI_1 = 1.2 \left[ 1.2(\rho_{NIR} - \rho_{green}) - 2.5(\rho_{red} - \rho_{green}) \right]$	[36]
Modified Triangular Vegetation Index 2 (MTVI <sub>2</sub> )	$MTVI_2 = \frac{1.5 \left[ 1(\rho_{NIR} - \rho_{green}) - 2.5(\rho_{red} - \rho_{green}) \right]}{\sqrt{2(\rho_{NIR} + 1)^2 - (6\rho_{NIR} - 5\sqrt{\rho_{red}}) - 0.5}}$	[36]
Modified Normalized Green–Red Difference Index (MNGRDI)	$MNGRDI = \frac{\rho_{green}^2 - \rho_{red}^2}{\rho_{green}^2 + \rho_{red}^2}$	[39]
Modified Soil-Adjusted Vegetation Index (MSAVI)	$MSAVI = 0.5 \left[ 2\rho_{NIR} + 1 - \sqrt{(2\rho_{NIR} + 1)^2 - 8(\rho_{NIR} - \rho_{red})} \right]$	[40]
Modified Simple Ratio (MSR)	$MSR = \frac{\left( \frac{\rho_{NIR}}{\rho_{red}} \right) - 1}{\sqrt{\left( \frac{\rho_{NIR}}{\rho_{red}} \right) + 1}}$	[41]
Normalised Difference Red Edge (NDRE)	$NDRE = \frac{\rho_{NIR} - \rho_{red\ edge}}{\rho_{NIR} + \rho_{red\ edge}}$	[42]
Normalised Difference Vegetation Index (NDVI)	$NDVI = \frac{\rho_{NIR} - \rho_{red}}{\rho_{NIR} + \rho_{red}}$	[43]
Normalized Green–Red Difference Index (NGRDI)	$NGRDI = \frac{\rho_{green} - \rho_{red}}{\rho_{green} + \rho_{red}}$	[44]
Optimised Soil Adjusted Vegetation Index-Green (OSAVI <sub>green</sub> )	$OSAVI_{green} = \frac{1.5(\rho_{green} - \rho_{red})}{(\rho_{green} + \rho_{red}) + 0.16}$	[35]
Renormalised Difference Vegetation Index (RDVI)	$RDVI = \sqrt{\frac{\rho_{NIR} - \rho_{red}}{\rho_{NIR} + \rho_{red}}}$	[45]
Simple Ratio (SR)	$SR = \frac{\rho_{NIR}}{\rho_{red}}$	[46]
Soil Adjusted Vegetation Index-Green (SAVI <sub>green</sub> )	$SAVI_{green} = \frac{(1+0.5) \times (\rho_{green} - \rho_{red})}{(\rho_{green} + \rho_{red}) + 0.5}$	[47]
Triangular Vegetation Index (TVI)	$TVI = 0.5 \left[ 120(\rho_{NIR} - \rho_{green}) - 200(\rho_{red} - \rho_{green}) \right]$	[48]

### 2.3. Obtaining the Morphological and Physiological Parameters

The a (ChlA<sub>leaf</sub>), b (ChlB<sub>leaf</sub>) and total (ChlT<sub>leaf</sub>) leaf chlorophyll indices were determined using a ClorofiLOG (model CFL 1030) digital device, collected on the same day as the RPA flights. The device provided indices proportional to the absorbance of chlorophyll. The readings were performed between 9 and 11 am using a fully expanded leaf located in the third or fourth node from the apex of the plagiotropic branch in the middle third of the plant. Only normal leaves and leaves not affected by any pests or diseases were considered. One plant was chosen per plot, totalling 90 analysed leaves.

The mean plant height (H) and crown diameter (D) of the four useful plants in each plot were measured using a metre ruler. Equation (1) was used to calculate the LAI, as described by [29]:

$$\text{LAI} = 0.0134 + 0.7276 \times D^2 \times H \quad (1)$$

The a (ChlA<sub>canopy</sub>), b (ChlB<sub>canopy</sub>), and total (ChlT<sub>canopy</sub>) canopy chlorophyll indices were determined from Equation (2) and according to the studies by [10,28]:

$$\text{Chl}_{\text{canopy}} = \text{Chl}_{\text{leaf}} \times \text{LAI} \quad (2)$$

#### 2.4. Meteorological Data

The monthly meteorological data of total rainfall (mm), minimum temperature (T<sub>min</sub>, in °C), maximum temperature (T<sub>max</sub>, in °C), and relative humidity (RH, in %) were obtained from the weather station of the National Institute of Meteorology (INMET, for its acronym in Portuguese), located at UFLA, from 1 November 2019 to 31 August 2021 (Figure 3). The wet season for Minas Gerais ranges from October to March, and the dry season goes from April to September.

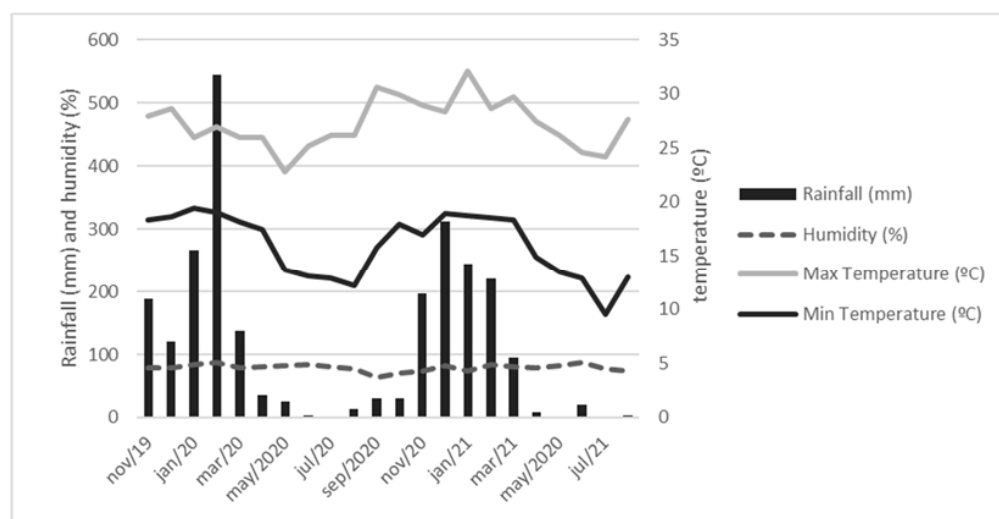


**Figure 3.** Graphical representation of the meteorological variables recorded monthly in Lavras, Minas Gerais, from November 2019 to August 2021.

#### 2.5. Statistical Analysis

Descriptive statistics (mean, median, maximum, minimum, and first and third quartiles) were calculated to support the exploratory data analysis. The data for ChlA<sub>leaf</sub>, ChlB<sub>leaf</sub>, ChlT<sub>leaf</sub>, ChlA<sub>canopy</sub>, ChlB<sub>canopy</sub>, and ChlT<sub>canopy</sub> were correlated with the 21 VIs using the Pearson correlation (R) for in the two study seasons. Student's *t* test was applied to evaluate whether the estimates were significant ( $p < 0.05$ ), and the residuals were calculated as the difference between the VI data estimated by the RPA images and the field measurements. The mean absolute error (MAE) and the root mean square error (RMSE) were also calculated. Further, the correlation between the Chl and VI data was analysed, which was significantly related in the first analysis to obtain the correlation coefficient (R). All the statistical analyses were performed in the statistical software R version 3.6.2 (R Core Team, Vienna, Austria).

### 3. Results

#### 3.1. Wet Season

Figure 4 shows that the correlation between H, D, LAI and Chl<sub>canopy</sub> and the VIs was positive and moderate, as indicated by the blue tones. Conversely, the correlation between the VIs and Chl<sub>leaf</sub> was negative. Moreover, the correlation between the Modified Chloro-

phyll Absorption Ratio Index 2 (MCARI2) VI and the morphological and physiological parameters was negative, as indicated by the red tones. In addition, the highest correlation between  $Chl_{leaf}$  and the VIs was weak and inverse ( $R = -0.26$ ). The highest correlation between the  $Chl_{canopy}$  and VIs was good and direct ( $R \leq 0.52$ ), except for the correlation between MCARI2 and  $Chl_{canopy}$  and  $Chl_{Tcanopy}$ , which was good but inverse ( $R = -0.51$ ). The correlation between Modified Chlorophyll Absorption Ratio Index 1 (MCARI1) and  $Chl_{leaf}$  and between the Modified Simple Ratio (MSR) and  $Chl_{leaf}$  was null or very weak ( $R = 0$ ).

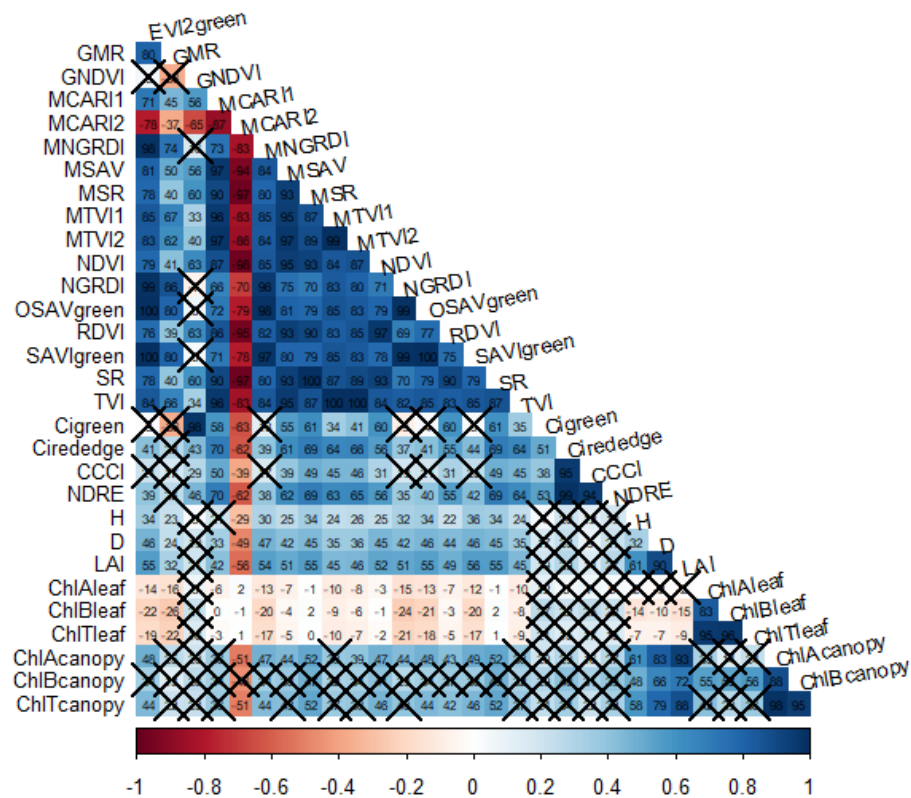


**Figure 4.** Correlation coefficients and non-significance of Student's *t* test (represented by ×) between the VIs and the morphophysiological parameters of coffee plants in the wet season (November 2019). The positive correlations are shown in blue, and the negative correlations are shown in red. Similarly, the strong correlations are in dark tones, and the weak correlations are in light tones.

Figure 4 also showed significant ( $p \leq 0.05$ ) and nonsignificant correlations ( $p > 0.05$ ). The “×” in Figure 4 represents a *p* value greater than the significance level set at 5%. The relationship between  $Chl_{Bcanopy}$  and the VIs was not significant. The VIs that were composed of the ratio of green and NIR (green normalised difference vegetation index (GNDVI) and green chlorophyll index (Cigreen)) and red edge and NIR (red-edge chlorophyll index (Cirededge), canopy chlorophyll content index (CCCI), and normalised difference red edge (NDRE)) were not related to the morphological parameters (H, D and LAI) or physiological parameters ( $Chl_{Aleaf}$ ,  $Chl_{Bleaf}$ ,  $Chl_{Tleaf}$ ,  $Chl_{Acanopy}$ ,  $Chl_{Bcanopy}$ , and  $Chl_{Tcanopy}$ ). Similarly, the correlations between green minus red (GMR) and  $Chl_{Acanopy}$ ,  $Chl_{Bcanopy}$  and  $Chl_{Tcanopy}$ ; between MCARI1 and the parameters H,  $Chl_{Acanopy}$ ,  $Chl_{Bcanopy}$  and  $Chl_{Tcanopy}$ ; between the modified soil-adjusted vegetation index (MSAVI) and  $Chl_{Bcanopy}$  and  $Chl_{Tcanopy}$ ; between modified triangular vegetation index 1 (MTVI1) and  $Chl_{Acanopy}$ ,  $Chl_{Bcanopy}$  and  $Chl_{Tcanopy}$ ; between modified triangular vegetation index 2 (MTVI2) and  $Chl_{Bcanopy}$  and  $Chl_{Tcanopy}$ ; between the normalised green–red difference index (NGRDI) and  $Chl_{Bcanopy}$  and  $Chl_{Tcanopy}$ ; and between the triangular vegetation index (TVI) and  $Chl_{Acanopy}$ ,  $Chl_{Bcanopy}$  and  $Chl_{Tcanopy}$  were not significant.

Given the results, this study considered only the analyses with significant variations ( $p \leq 0.05$ ) and with a positive (direct) and/or negative (inverse) correlation coefficient greater than 0.50. Therefore, the relationships between  $\text{Chl}_{\text{canopy}}$  and the MCARI2RPA, MSRRPA, and Simple Ratio (SRRPA) were analysed, and these VIs were statistically adequate to explain the Chl inversion method.

As observed in Figure 5, MCARI2RPA, MSRRPA, and SRRPA were not highly correlated with  $\text{Chl}_{\text{leaf}}$ , as values of  $R = 0.02$  and  $R^2 = 0.01$  were found for MCARI2RPA and  $R = -0.01$  and  $R^2 = -0.01$  for RSMRPA and SRRPA.

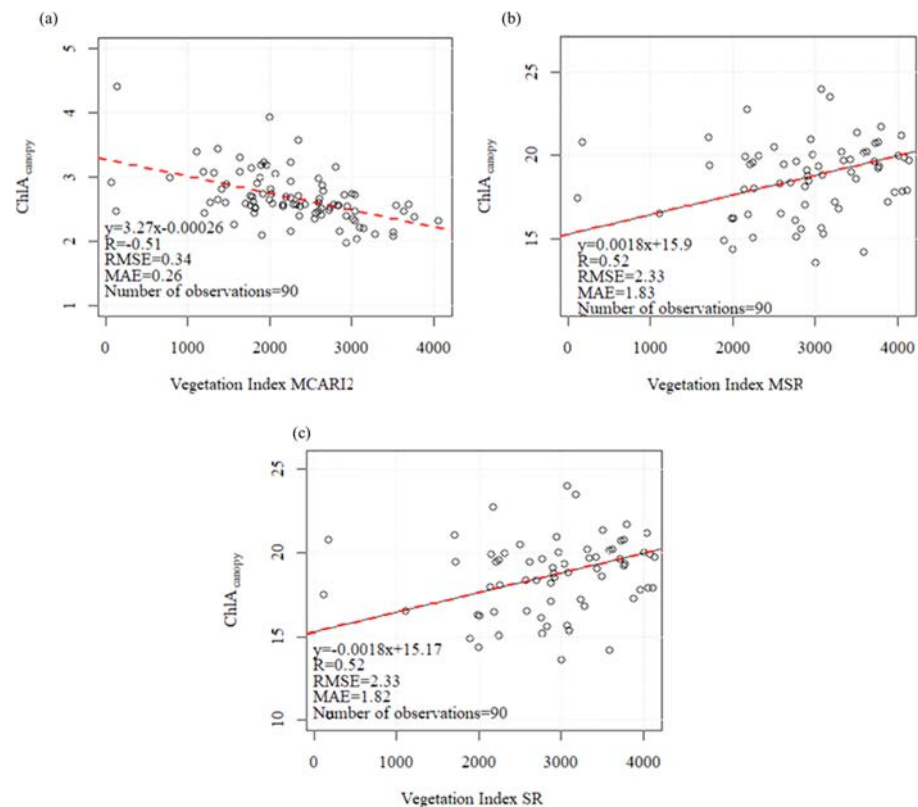


**Figure 5.** Relationship between (a) MCARI2RPA and measurements of the chlorophyll a content in the canopy ( $\text{ChlA}_{\text{canopy}}$ ); (b) RSMRPA and  $\text{ChlA}_{\text{canopy}}$ ; (c) SRRPA and  $\text{ChlA}_{\text{canopy}}$ .

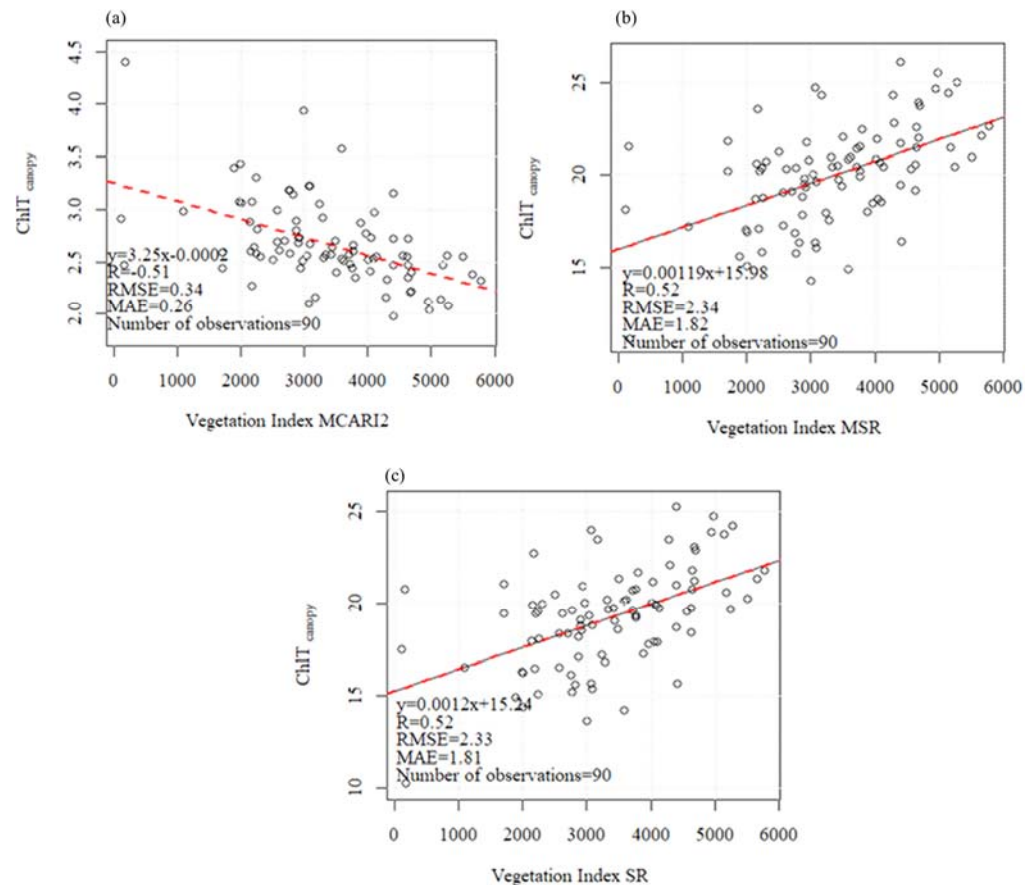
Figure 5 presents the regression relationship between MCARI2RPA, MSRRPA and SRRPA and  $\text{Chl}_{\text{canopy}}$  improved considerably when using the Chl inversion method. The correlation coefficient between MCARI2RPA and  $\text{Chl}_{\text{leaf}}$  changed from  $R = 0.01$  to  $R = -0.51$  (Figure 6a), and the coefficient of determination changed from  $R^2 = -0.01$  to  $R^2 = 0.26$ . The correlation coefficients between RSMRPA and  $\text{Chl}_{\text{leaf}}$  (Figure 6b) changed from  $R = 0.00$  to  $R = 0.52$ , and those between SRRPA and  $\text{Chl}_{\text{leaf}}$  (Figure 6c) change from  $R = 0.01$  to  $R = 0.52$ . The coefficient of determination changed from  $R^2 = -0.01$  to  $R^2 = 0.26$  in both relationships, going from a null relationship to a significant ( $p \leq 0.05$ ) and nonzero correlation.

The RMSE and MAE values demonstrated good performance in estimating Chl from the VIs studied and MSRRPA and SRRPA showed higher RMSE and MAE values than MCARI2RPA (Figure 6).

The error or residuals were calculated for each correlated data point to evaluate the regression model's effectiveness. Figure 7 shows the dispersion of the residuals is in accordance with the regression assumptions, in which the residuals should be randomly distributed around zero.

In Figure 8a, MCARI2RPA has an inverse relationship; the soil is represented in yellow, and the vegetation in blue and purple. This index showed a negative correlation with Chl.

Different results were found by [36], who observed a positive correlation between MCARI2 and Chl in maize and wheat. This result can be attributed to different spectral behaviour variations between crops.



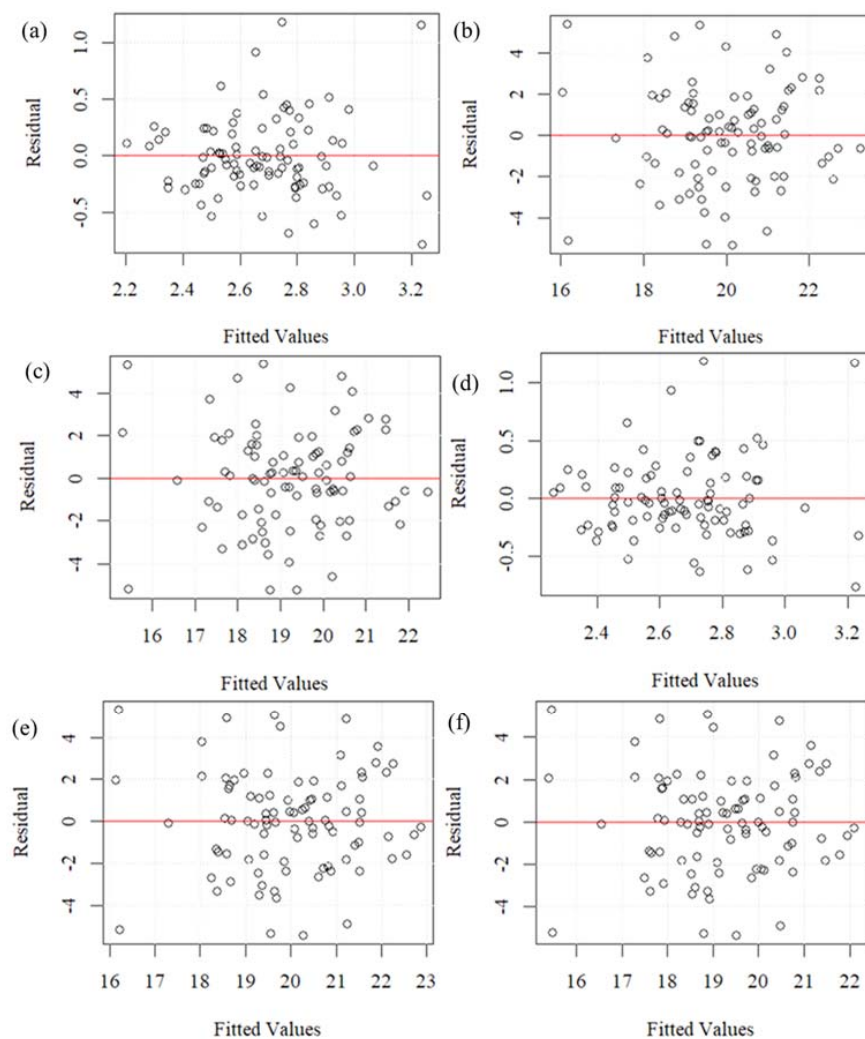
**Figure 6.** Relationship between (a) MCARI2RPA and measurements of total chlorophyll content in the canopy (ChlTcanopy); (b) MSRRPA and ChlTcanopy; (c) SRRPA and ChlTcanopy.

Figure 8b,c show the similarity in the characterisation and variability of RSMRPA and SRRPA. Note that the highest VI values are represented in green and the soil in purple; in addition, there is variability in the VIs between the treatments.

### 3.2. Dry Season

For the 2020 dry season, the correlations between H, LAI and  $Chl_{canopy}$  and the VIs were positive and weak. The correlations between D and the VIs and between  $Chl_{leaf}$  and the VIs were positive and moderate, as indicated by the more intense blue tones in Figure 9. The correlations between D and the CCCI vegetation index and between  $Chl_{leaf}$  and this index were negative and weak, as indicated by the light red tones. The relationships between H, LAI and  $Chl_{canopy}$  and CCCI were not significant. In the figure, x represents a  $p$  value greater than the significance level of 5% (Figure 9).

For the 2021 dry season, the correlations between H, D, LAI,  $Chl_{canopy}$  and the VIs were negative and weak, as indicated by light red tones in Figure 10. The correlations between  $Chl_{leaf}$  and the VIs were not significant. The same fact was observed in the correlation between H and CCCI (Figure 10).



**Figure 7.** Residuals of the values estimated by the VIRPA and the parameters measured in the field: (a) MCARI2RPA and ChlAcanopy, (b) MSRRPA and ChlAcanopy, (c) SRRPA and ChlAcanopy, (d) MCARI2RPA and ChlTcanopy, (e) MSRRPA and ChlTcanopy, and (f) SRRPA and ChlTcanopy.

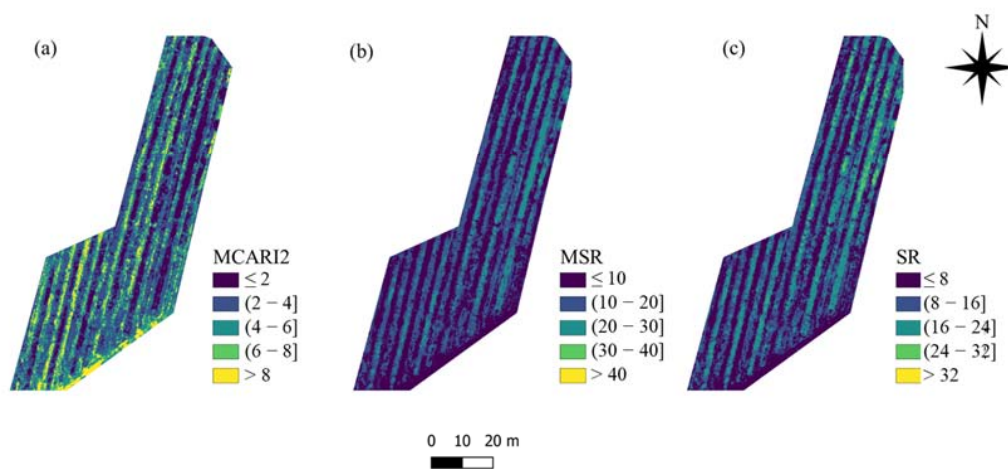


**Figure 8.** Maps produced from the vegetation indices for the study site: (a) MCARI2RPA; (b) MSRRPA; (c) SRRPA.



## 4. Discussion

### 4.1. Wet Season

In this study, a correlation was made between the VIs and the morphophysiological parameters of coffee plants in the wet season (November 2019), presented in Figure 4 of Section 3.1. Similar results were found by [49]. These authors studied the ChlTleaf estimate using radiometric data of the VIs obtained from an RPA in a recently transplanted coffee plantation (*Coffea arabica* L.) with the cultivars Catucaí (2SL), Catucaí (IAC 62), and Bourbon (IAC J10) and an age of 5 months at the beginning of the study, as the results were not significant for the studied variable.

Although [49] followed the method to measure the leaf chlorophyll content, the results found were due to the ability to measure and estimate the VIs obtained from RPA images since the data obtained from images represented the chlorophyll content of the canopy, whereas the measurements that were correlated represented the measurement of a single leaf in a given plant. In addition, the method used should be considered, as the correlation can be improved by using other methods for obtaining Chl. Another way that the calculation of Chl can be improved may be by measuring different parts and sides of the plant.

Another factor that may have contributed to this result is the age of the coffee trees under study, as the coffee plants were 3 years old at the time of collection. The authors of [5] investigated an algorithm to predict the Chl content in coffee plants using Sentinel-2 data at different spatial resolutions and different plant ages. The results showed that the best modelling results ( $R^2 = 0.69$ , RMSE = 6.8) were achieved when all bands were used at 10 m spatial resolution in the modelling of Chl for all coffee plants. The prediction accuracy improved ( $R^2 = 0.77$ , RMSE = 5.9) when only coffee plants aged between 5 and 8 years were considered.

However, the results found in the present study improved considerably when ChlAleaf was multiplied by the LAI using the Chl inversion method in the wet season. The correlation coefficient changed from  $R = 0.02$  to  $R = -0.51$  and the coefficient of determination changed from  $R^2 = -0.01$  to  $R^2 = 0.26$  for the relationship between MCARI2RPA and ChlAleaf (Figure 5a). Conversely, the correlation coefficients between MSRRPA and ChlAleaf (Figure 5b) and between SRRPA and ChlAleaf (Figure 5c) changed from  $R = -0.01$  to  $R = 0.52$ , and the coefficient of determinations changed from  $R^2 = -0.01$  to  $R^2 = 0.26$  in these two relationships, going from a null relationship to a significant ( $p \leq 0.05$ ) and nonzero correlation.

Similar results were obtained by [10], who used the LAI to map the chlorophyll content in maize using RPA images and obtained a high correlation between the VI NDRE and the canopy chlorophyll, calculated by multiplying  $Chl_{leaf}$  and the LAI. In that study, the coefficient of determination increased from  $R^2 = 0.177$  to  $R^2 = 0.774$  when the canopy chlorophyll content was calculated using the LAI.

The spectral bands used in this study that showed statistically significant values were the NIR, red, and green bands. According to [36], the MSR and SR showed an improvement in the images concerning sensitivity, and the linear relationship with the vegetation morphological parameters, whereas MCARI2 is less sensitive to changes in chlorophyll content and linearly related to the LAI. It should be noted that in the study by [10], the authors used the red edge band in maize, which shows the importance of evaluating the method in different crops since each crop has its own unique spectral characteristics.

According to [36], MCARI2RPA, MSRRPA, and SRRPA have high sensitivity and, therefore, are more affected by variability in chlorophyll. According to the same authors, this is because the formulas of the VIs take into account the red, green and NIR bands, which are bands highly correlated with  $Chl_{leaf}$  and  $Chl_{canopy}$ .

### 4.2. Dry Season

For both dry season days studied, there were no patterns in the relationships between  $Chl_{leaf}$ ,  $Chl_{canopy}$  and the VIs. In the 2020 dry season, the correlation between  $Chl_{leaf}$

and the VIs was greater than the correlation between  $\text{Chl}_{\text{canopy}}$  and the VIs. In the 2021 dry season, the correlations between  $\text{Chl}_{\text{leaf}}$  and the VIs were not significant, and the correlations between  $\text{Chl}_{\text{canopy}}$  and the VIs were negative and weak. These results were the inverse of those found for the 2019 wet season and can be attributed to climatic variations (Figure 3), mainly in rainfall and temperature, as in the dry season, the crop experienced a water deficit due to the low rain.

Some studies evaluating plants in situations of water deficit have observed that the chlorophyll content increased with a decrease in the volumetric water content in the soil [50,51]. Conversely, [52] observed that coffee plants grown in winter and growing under water stress showed no changes in chlorophyll content.

Although the Chl inversion method is not new, this study explores the impact of high-spatial-resolution RPA images in obtaining Chl maps of coffee plants using VIs. Therefore, in agriculture and especially in precision coffee farming, these applications are valid since rapid phenological changes occur that can be monitored with this technology.

Given the results found in the dry season and because obtaining effective results on the relationship between  $\text{Chl}_{\text{leaf}}$ ,  $\text{Chl}_{\text{canopy}}$  and VIs is an incipient topic in coffee growing, there is a need for studies to evaluate these relationships between chlorophyll and VIs.

We recommend that in future studies this method be applied to different cultivars and different water deficiency levels and that other VIs that may produce better results be evaluated. It is important to note that the studied method should consider the specificities of the canopy structure, the time of data collection, the light on the day of data acquisition, the sensor used, the calibration, and the image processing. Thus, when using this approach to apply VIs in a generalised manner to a given crop, compiling a database of acquired images is recommended, covering a wide range of the factors mentioned above. In addition, field data must be collected to validate the method in different seasons. Another recommendation is to perform studies investigating the correlation of visible bands with Chl values since if the visible bands interact with ChlA and ChlB, low-cost RPA can be used to obtain and estimate these parameters using this technology.

## 5. Conclusions

The challenge for coffee producers is to obtain chlorophyll content data in a timely manner to apply nutritional control measures. Currently equipment, such as chlorophyll metres, is used to obtain field data. The availability of high spatial resolution RPA images combined with digital image processing and VI allows the detection of plant nutritional information, allowing for faster and more proactive monitoring and decision making.

In this study, we identified which VIs adequately explained the Chl inversion method and evaluated the relationships between VIs obtained from RPA images and the  $\text{Chl}_{\text{leaf}}$  and  $\text{Chl}_{\text{canopy}}$  indices of coffee trees in the wet and dry seasons.

The results of this study suggest that it is possible to use the Chl inversion method for images of coffee plants trees obtained by RPA during the wet season. The relationships between the  $\text{MCARI2}_{\text{RPA}}$ ,  $\text{MSR}_{\text{RPA}}$  and  $\text{SR}_{\text{RPA}}$  VIs were appropriate for estimating  $\text{Chl}_{\text{canopy}}$  in the wet season.

For both dry seasons studied, there were no patterns in the relationships between  $\text{Chl}_{\text{leaf}}$ ,  $\text{Chl}_{\text{canopy}}$ , and the studied VIs. Given the results found in the dry season and because obtaining effective results on the relationships between  $\text{Chl}_{\text{leaf}}$ ,  $\text{Chl}_{\text{canopy}}$  and VIs is an incipient topic in coffee growing, there is a need for future studies to evaluate the relationships between chlorophyll and VIs.

The results found in this paper reinforce the use of RPA to obtain images of a coffee field. Furthermore, these collected images can be analysed through VIs, which can result in the observation of the spatial variability of chlorophyll in an area. Therefore, works such as this can be replicated by producers, technicians, and scientists to understand the behaviour of this variable in a coffee field, mainly in the wet season.

**Author Contributions:** Conceptualisation, L.M.d.S. and G.A.e.S.F.; methodology, L.M.d.S.; software, L.M.d.S.; formal analysis, L.M.d.S., investigation, L.M.d.S., G.A.e.S.F., M.A.d.F.C., S.A.T., A.A.V.C. and P.M.N.; resources, L.M.d.S.; data curation, L.M.d.S., S.A.T., A.A.V.C. and P.M.N.; writing—original draft preparation, L.M.d.S.; writing—review and editing, G.A.e.S.F. and M.A.d.F.C.; visualisation, G.A.e.S.F. and M.A.d.F.C.; supervision, G.A.e.S.F. and M.A.d.F.C.; project administration, L.M.d.S., G.A.e.S.F. and M.A.d.F.C.; funding acquisition, G.A.e.S.F. and M.A.d.F.C. All authors have read and agreed to the published version of the manuscript.

**Funding:** This research was funded by the Embrapa Café—Consórcio Pesquisa Café, project no. 10.18.20.041.00.00, the National Council for Scientific and Technological Development (CNPq), project no. 305953/2020-6, the Coordination for the Improvement of Higher Education Personnel (CAPES) and the Federal University of Lavras (UFLA).

**Institutional Review Board Statement:** Not applicable.

**Informed Consent Statement:** Not applicable.

**Data Availability Statement:** Not applicable.

**Acknowledgments:** The authors acknowledge the Federal University of Lavras (UFLA) and the Graduate Program in Agricultural Engineering (PPGEA) for supporting this study; Consórcio Pesquisa Café (project no. 10.18.20.041.00.00)—Embrapa Coffee for funding the research; and the National Council for Scientific and Technological Development (CNPq) (project no. 305953/2020-6), Minas Gerais Research Foundation (Fundação de Amparo à Pesquisa do Estado de Minas Gerais—FAPEMIG) and Coordination for the Improvement of Higher Education Personnel (CAPES) for the financial support. We also thank the Coffee Sector of UFLA, NESA and NECAF for supporting the development of the study.

**Conflicts of Interest:** The authors declare no conflict of interest.

## References

1. United States Department of Agriculture (USDA). Available online: <http://usda.mannlib.cornell.edu/MannUsda/viewDocumentInfo?documentID=1801> (accessed on 1 July 2022).
2. De Souza, A.J.J.; Guimarães, R.J.; Colombo, A.; Sant’ana JA, D.V.; Castanheira, D.T. Quantitative analysis of growth in coffee plants cultivated with a water-retaining polymer in an irrigated system1. *Rev. Ciência Agronômica* **2016**, *47*, 162–171.
3. Pozza, E.A.; Carvalho, V.L.; Chalfoun, S.M. Sintomas de injúrias causadas por doenças do cafeeiro. In *Semiologia do Cafeeiro: Sintomas de Desordens Nutricionais, Fitossanitárias e Fisiológicas*; Guimarães, R.J., Mendes, A.N.G., Baliza, D.P., Eds.; UFLA: Lavras, Brazil, 2010.
4. Marin, D.B.; De Alves, M.C.; Pozza, E.A.; Belan, L.L.; De Freitas, M.L.O. Multispectral radiometric monitoring of bacterial blight of coffee. *Precis. Agric.* **2019**, *20*, 959–982. [[CrossRef](#)]
5. Chemura, A.; Mutanga, O.; Odindi, J. Empirical modeling of leaf chlorophyll content in coffee (*cofea arabica*) plantations with sentinel-2 msi data: Effects of spectral settings, spatial resolution, and crop canopy cover. *IEEE J. Sel. Top. Appl. Earth Obs. Remote Sens.* **2017**, *10*, 5541–5550. [[CrossRef](#)]
6. Santos, L.M.; De Barbosa, B.D.S.; Diotto, A.V.; Maciel, D.T.; Xavier, L.A.G. Biophysical parameters of coffee crop estimated by UAV RGB images. *Precis. Agric.* **2020**, *21*, 1227–1241. [[CrossRef](#)]
7. Santos, L.M.; De Barbosa, B.D.S.; Diotto, A.V.; Andrade, M.T.; Conti, L.; Rossi, G. Determining the Leaf Area Index and Percentage of Area Covered by Coffee Crops Using UAV RGB Images. *IEEE J. Sel. Top. Appl. Earth Obs. Remote Sens.* **2020**, *13*, 6401–6409. [[CrossRef](#)]
8. Putra, B.T.W.; Soni, P. Enhanced broadband greenness in assessing Chlorophyll a and b, Carotenoid, and Nitrogen in Robusta coffee plantations using a digital camera. *Precis. Agric.* **2018**, *19*, 238–256. [[CrossRef](#)]
9. Moreira, M.A. *Fundamentos do Sensoriamento Remoto e Metodologias de Aplicação*; UFV: Viçosa, Brazil, 2012.
10. Milas, A.S.; Romanko, M.; Reil, P.; Abeyasinghe, T.; Marambe, A. The importance of leaf area index in mapping chlorophyll content of corn under different agricultural treatments using UAV images. *Int. J. Remote Sens.* **2018**, *39*, 5415–5431. [[CrossRef](#)]
11. Santos, P.L.F.; Castilho, R.M.M.; Gazola, R.P.D. Pigmentos fotossintéticos e sua correlação com nitrogênio e magnésio foliar em grama bermuda cultivada em substratos. *Acta Iguazu* **2019**, *8*, 92–101.
12. Han, L.; Yang, G.; Dai, H.; Xu, B.; Yang, H.; Feng, H.; Li, Z.; Yang, X. Modeling maize above-ground biomass based on machine learning approaches using UAV remote-sensing data. *Plant Methods* **2019**, *15*, 1–19. [[CrossRef](#)]
13. Formaggio, A.R.; Sanches, I.D. *Sensoriamento Remoto em Agricultura*; Oficina de Textos: São Paulo, Brazil, 2017; 288p.
14. Streit, N.M.; Canterle, L.P.; Canto MW, D.; Hecktheuer LH, H. As clorofilas. *Ciência Rural* **2005**, *35*, 748–755. [[CrossRef](#)]
15. Zhang, H.; Liang, J.; Luo, Y.; Tang, N.; Li, X.; Zhu, Z.; Guo, J. Comparative effects of polystyrene nanoplastics with different surface charge on seedling establishment of Chinese cabbage (*Brassica rapa* L.). *Chemosphere* **2022**, *292*, 133403. [[CrossRef](#)] [[PubMed](#)]

16. Salami, E.; Barrado, C.; Pastor, E. UAV Flight Experiments Applied to the Remote Sensing of Vegetated Areas. *Remote Sens.* **2014**, *6*, 11051–11081. [[CrossRef](#)]
17. Santos, L.M.; Ferraz, G.A.S.; Barbosa, B.D.S.; Andrade, A.D. Use of remotely piloted aircraft in precision agriculture: A review. *Dyna* **2019**, *86*, 284–291.
18. Emilien, A.V.; Thomas, C.; Thomas, H. UAV & satellite synergies for optical remote sensing applications: A literature review. *Sci. Remote Sens.* **2021**, *3*, 100019.
19. Matese, A.; Toscano, P.; Di Gennaro, S.F.; Genesio, L.; Vaccari, F.P.; Primicerio, J.; Gioli, B. Intercomparison of UAV, aircraft and satellite remote sensing platforms for precision viticulture. *Remote Sens.* **2015**, *7*, 2971–2990. [[CrossRef](#)]
20. Jacquemoud, S.; Verhoef, W.; Baret, F.; Bacour, C.; Zarco-Tejada, P.J.; Asner, G.P.; François, C.; Ustin, S.L. PROSPECT+ SAIL models: A review of use for vegetation characterisation. *Remote Sens. Environ.* **2009**, *113*, S56–S66. [[CrossRef](#)]
21. Upreti, D.; Huang, W.; Kong, W.; Pascucci, S.; Pignatti, S.; Zhou, X.; Ye, H.; Casa, R. A Comparison of Hybrid Machine Learning Algorithms for the Retrieval of Wheat Biophysical Variables from Sentinel-2. *Remote Sens.* **2019**, *11*, 481. [[CrossRef](#)]
22. Meroni, M.; Colombo, R.; Panigada, C. Inversion of a radiative transfer model with hyperspectral observations for LAI mapping in poplar plantations. *Remote Sens. Environ.* **2004**, *92*, 195–206. [[CrossRef](#)]
23. Richter, K.; Atzberger, C.; Vuolo, F.; Weihs, P.; D’urso, G. Experimental assessment of the Sentinel-2 band setting for RTM-based LAI retrieval of sugar beet and maize. *Can. J. Remote Sens.* **2014**, *35*, 230–247. [[CrossRef](#)]
24. Palacharla, P.K.; Durbha, S.S.; King, R.L.; Gokaraju, B.; Lawrence, G.W. A hyperspectral reflectance data based model inversion methodology to detect reniform nematodes in cotton. In Proceedings of the 6th International Workshop on the Analysis of Multi-Temporal Remote Sensing Images (Multi-Temp), Trento, Italy, 12 July 2011.
25. Le Maire, G.; Marsden, C.; Verhoef, W.; Ponzoni, F.J.; Seen, D.L.; Bégué, A.; Stape, J.-L.; Nouvellon, Y. Leaf area index estimation with MODIS reflectance time series and model inversion during full rotations of Eucalyptus plantations. *Remote Sens. Environ.* **2011**, *115*, 586–599. [[CrossRef](#)]
26. Si, Y.; Schlerf, M.; Zurita-Milla, R.; Skidmore, A.; Wang, T. Mapping spatio-temporal variation of grassland quantity and quality using MERIS data and the PROSAIL model. *Remote Sens. Environ.* **2012**, *121*, 415–425. [[CrossRef](#)]
27. Wang, Z.; Skidmore, A.K.; Darvishzadeh, R.; Wang, T. Mapping Forest canopy nitrogen content by inversion of coupled leaf-canopy radiative transfer models from airborne hyperspectral imagery. *Agric. For. Meteorol.* **2018**, *253*, 247–260. [[CrossRef](#)]
28. Liang, L.; Qin, Z.; Zhao, S.; Di, L.; Zhang, C.; Deng, M.; Lin, H.; Zhang, L.; Wang, L.; Liu, Z. Estimating crop chlorophyll content with hyperspectral vegetation indices and the hybrid inversion method. *Int. J. Remote Sens.* **2016**, *37*, 2923–2949. [[CrossRef](#)]
29. Favarin, J.L.; Neto, D.D.; García, Y.; García, A.; Nova, N.A.V.; Favarin, M.D.G.G.V. Equações para a estimativa do índice de área foliar do cafeeiro. *Pesqui. Agropecuária Bras.* **2002**, *37*, 769–773. [[CrossRef](#)]
30. Ahmad, A.; Ordoñez, J.; Cartujo, P.; Martos, V. Remotely Piloted Aircraft (RPA) in Agriculture: A Pursuit of Sustainability. *Agronomy* **2021**, *11*, 7. [[CrossRef](#)]
31. Castanheira, D.T.; Barcelos, T.R.; Guimarães, R.J.; Carvalho, M.A.D.F.; Rezende, T.T.; Bastos, I.D.S.; Cruvinel, A.H. Agronomic techniques for mitigating the effects of water restriction on coffee crops. *Coffee Sci.* **2019**, *14*, 104–115. [[CrossRef](#)]
32. Alecrim, A.O.; Castanheira, D.T.; Voltolini, G.B.; Netto, P.M.; Guimarães, R.J.; Gonçalves, A.H. Phytosociology of weeds in coffee plants with different soil management techniques. *Scientia Agrar. Parana.* **2020**, *19*, 270–279. [[CrossRef](#)]
33. Eitel, J.U.H.; Keefe, R.F.; Long, D.S.; Davis, A.S.; Vierling, L.A. Active ground optical remote sensing for improved monitoring of seedling stress in nurseries. *Sensors* **2010**, *10*, 2843–2850. [[CrossRef](#)]
34. Rundquist, D.C.; Gitelson, A.A.; Viña, A.; Arkebauer, T.J.; Keydan, G.; Leavitt, B. Remote estimation of leaf area index and green leaf biomass in maize canopies. *Geophys. Res. Lett.* **2003**, *30*, 52-1–52-4.
35. Putra, B.T.W.; Soni, P. Evaluating NIR-Red and NIR-Red edge external filters with digital cameras for assessing vegetation indices under different illumination. *Infrared Phys. Technol.* **2017**, *81*, 148–156. [[CrossRef](#)]
36. Haboudane, D.; Miller, J.R.; Pattey, E.; Zarco-Tejada, P.J.; Strachan, I.B. Hyperspectral vegetation indices and novel algorithms for predicting green LAI of crop canopies: Modeling and validation in the context of precision agriculture. *Remote Sens. Environ.* **2004**, *90*, 337–352. [[CrossRef](#)]
37. Wang, Y.; Wang, D.; Zhang, G.; Wang, J. Estimating nitrogen status of rice using the image segmentation of G-R thresholding method. *Field Crops Res.* **2013**, *149*, 33–39. [[CrossRef](#)]
38. Gitelson, A.A.; Merzlyak, M.N. Signature analysis of leaf reflectance spectra: Algorithm development for remote sensing of chlorophyll. *J. Plant Physiol.* **1996**, *148*, 494–500. [[CrossRef](#)]
39. Bendig, J.; Kang, Y.; Aasen, H.; Bolten, A.; Bennertz, S.; Broscheit, J.; Gnyp, M.L.; Bareth, G. Combining UAV-Based Plant Height from Crop Surface Models, Visible, and near Infrared Vegetation Indices for Biomass Monitoring in Barley. *Int. J. Appl. Earth Obs. Geoinf.* **2015**, *39*, 79–87. [[CrossRef](#)]
40. Qi, J.; Chehbouni, A.; Huete, A.R.; Kerr, Y.H.; Sorooshian, S. A modified soil adjusted vegetation index. *Remote Sens. Environ.* **1994**, *48*, 119–126. [[CrossRef](#)]
41. Chen, J.M. Evaluation of vegetation indices and a modified simple ratio for boreal applications. *Can. J. Remote Sens.* **1996**, *22*, 229–242. [[CrossRef](#)]

42. Barnes, E.M.; Clarke, T.R.; Richards, S.E.; Colaizzi, P.D.; Haberland, J.; Kostrzewski, M.; Waller, P.; Choi, C.; Riley, E.; Thompson, T.; et al. Coincident detection of crop water stress, nitrogen status and canopy density using ground based multispectral data. In Proceedings of the 5th International Conference on Precision Agriculture, Bloomington, MN, USA, 19 July 2000.
43. Rouse, J.W.; Haas, R.H.; Schell, J.A.; Deering, D.W. Monitoring vegetation systems in the Great Plains with ERTS. *Goddard Spec. Flight Cent. NASA* **1976**, *24*, 309–317.
44. Tucker, C.J. Red and photographic infrared linear combinations for monitoring vegetation. *Remote Sens. Environ.* **1979**, *8*, 127–150. [[CrossRef](#)]
45. Roujean, J.-L.; Breon, F.-M. Estimating PAR Absorbed by Vegetation from Bidirectional Reflectance Measurements. *Remote Sens. Environ.* **1995**, *51*, 375–384. [[CrossRef](#)]
46. Birth, G.S.; Mcvey, G.R. Measuring the color of growing turf with a reflectance spectrophotometer. *Agron. J.* **1968**, *60*, 640–643. [[CrossRef](#)]
47. Li, Y.; Chen, D.; Walker, C.N.; Angus, J.F. Estimating the nitrogen status of crops using a digital camera. *Field Crops Res.* **2010**, *118*, 221–227. [[CrossRef](#)]
48. Broge, N.H.; Leblanc, E. Comparing prediction power and stability of broadband and hyperspectral vegetation indices for estimation of green leaf area index and canopy chlorophyll density. *Remote Sens. Environ.* **2000**, *76*, 156–172. [[CrossRef](#)]
49. Bento, N.L.; Ferraz, G.A.E.S.; Barata, R.A.P.; Soares, D.V.; Santos, L.M.D.; Santana, L.S.; Palchetti, E. Characterization of Recently Planted Coffee Cultivars from Vegetation Indices Obtained by a Remotely Piloted Aircraft System. *Sustainability* **2022**, *14*, 1446. [[CrossRef](#)]
50. Pereira, T.B.; Baliza, D.P.; Cunha, R.L.; Guimarães, R.J.; Gomes, R.A.; Pereira, V.A. Teores de clorofila em cafeeiros submetidos a diferentes ambientes avaliados por dois métodos de determinação. In Proceedings of the Simpósio de Pesquisa dos Cafés do Brasil, Araxá, MG, Brazil, 22 August 2011.
51. Yin, C.Y.; Pang, X.Y.; Peuke, A.D.; Wang, X.; Chen, K.; Gong, R.G. Growth and photosynthetic responses in *Jatropha curcas* L. seedlings of different provenances to watering regimes. *Photosynthetica* **2016**, *54*, 367–373. [[CrossRef](#)]
52. Alonso Zuñiga, E.; Ruiz Machuca, L.M.; Dos Santos, O.F.; De Souza, C.M.L.; De Oliveira, F.D.P.; Broetto, F. Comportamento fisiológico de mudas de cafeeiro arábica (cv. Obatã e catucaí) submetidas à deficiência hídrica. *Irriga* **2019**, *24*, 890–899. [[CrossRef](#)]